CT prediction of the Fuhrman grade of clear cell renal cell carcinoma (RCC): towards the development of computer-assisted diagnostic method

Hannu Huhdanpaa [ORCID],[1] Darryl Hwang,[1] Steven Cen,[1] Brian Quinn,[1] Megha Nayyar,[1] Xuejun Zhang,[2] Frank Chen,[1] Bhushan Desai,[1] Gangning Liang,[3] Inderbir Gill,[3] Vinay Duddalwar[1]

[1]Department of Radiology, University of Southern California, 1500 San Pablo St, 2nd floor imaging, Los Angeles, CA 90033, USA
[2]Viterbi School of Engineering, University of Southern California, Los Angeles, USA
[3]Department of Urology, University of Southern California, 1441 Eastlake Ave, NOR 7416, Los Angeles, CA 9003, USA

Abstract

Purpose: There are distinct quantifiable features characterizing renal cell carcinomas on contrast-enhanced CT examinations, such as peak tumor enhancement, tumor heterogeneity, and percent contrast washout. While qualitative visual impressions often suffice for diagnosis, quantitative metrics if developed and validated can add to the information available from standard of care diagnostic imaging. The purpose of this study is to assess the use of quantitative enhancement metrics in predicting the Fuhrman grade of clear cell RCC.

Materials and methods: 65 multiphase CT examinations with clear cell RCCs were utilized, 44 tumors with Fuhrman grades 1 or 2 and 21 tumors with grades 3 or 4. After tumor segmentation, the following data were extracted: histogram analysis of voxel-based whole lesion attenuation in each phase, enhancement and washout using mean, median, skewness, kurtosis, standard deviation, and interquartile range.

Results: Statistically significant difference was observed in 4 measured parameters between grades 1–2 and grades 3–4: interquartile range of nephrographic attenuation values, standard deviation of absolute enhancement, as well as interquartile range and standard deviation of residual nephrographic enhancement. Interquartile range of nephrographic attenuation values was 292.86 HU for grades 1–2 and 241.19 HU for grades 3–4 (p value 0.02). Standard deviation of absolute enhancement was 41.26 HU for grades 1–2 and 34.66 HU for grades 3–4 (p value 0.03). Interquartile range was 297.12 HU for residual nephrographic enhancement for grades 1–2 and 235.57 HU for grades 3–4 (p value 0.02), and standard deviation of the same was 42.45 HU for grades 1–2 and 37.11 for grades 3–4 (p value 0.04).

Conclusion: Our results indicate that absolute enhancement is more heterogeneous for lower grade tumors and that attenuation and residual enhancement in nephrographic phase is more heterogeneous for lower grade tumors. This represents an important step in devising a predictive non-invasive model to predict the nucleolar grade.

Key words: Renal cell carcinoma—Quantitative imaging—Computer-assisted diagnosis—Computed tomography (CT)

Renal cancer accounts for more than 2% of cancers in humans worldwide [1]. In the United States, the annual incidence of renal cancer increased yearly by 1.6% over the past decade, with over 63,000 new cases in 2014 [2]. A majority of renal tumors are incidentally diagnosed on medical imaging, being often asymptomatic, small in size, and early stage [3, 4].

The importance of the work presented here is in the context of active surveillance (AS) [4]. If a lower grade tumor can be radiologically diagnosed with confidence, the impact on clinical management decision-making in these patients will be significant. It may substitute the need for a percutaneous renal biopsy, if considered, but will also provide more information that will be useful if active surveillance is considered as a management option [5], particularly for patients with small renal masses (<4 cm) and elderly patients or patients with significant comorbidities. As AS requires strong patient commitment, as well as imaging follow-up, having this information while management options are discussed with patients is very helpful. Additionally, it will also help in providing prognostic information and therefore help in building a personalized cancer model for the patient.

There are distinct quantifiable features characterizing renal cell carcinomas (RCC) on contrast-enhanced CT (CECT) examinations, such as peak tumor enhancement, tumor heterogeneity, and percent contrast washout [6–13]. Qualitative impressions based on visual inspections of the images are frequently sufficient for making major clinical management decisions.

Prior studies have demonstrated the degree of CT enhancement as a potentially valuable parameter in differentiating between RCC subtypes [6]. The purpose of this study is to focus on a specific subtype, clear cell RCC, and assess whether quantitative attenuation, enhancement, and washout metrics may be used to predict the Fuhrman grade of clear cell RCC.

The Fuhrman grading system is widely used for histologic grade stratification of RCC on the basis of nuclear size and shape, as well as the prominence of nucleoli [14]. The original grading system had 4 grades: grade 1 with small, round, uniform nuclei, inconspicuous nucleoli; grade 2 (40% of tumors) with slightly irregular nuclei, nuclear diameter of 15 microns and open chromatin; grade 3 (30%–40% of tumors) with very irregular nuclei, nuclear diameter of 20 microns and open chromatin; and grade 4 (15% of tumors) with mitoses, bizarre, multilobulated, pleomorphic cells, and macronucleoli, in addition to grade 3 features.

Several studies [15–20] have shown that the original moderate intra- and interobserver agreement among pathologists is improved to substantial agreement when the Fuhrman grading system is collapsed to two categories where Fuhrman grades 1 and 2 are considered together as low grade and Fuhrman grades 3 and 4 are considered together as high grade.

More recently, with an aim to improve interobserver variation, International Society of Urological Pathology (ISUP) grading system of RCCs has been developed, based on tumor cell nucleolar prominence [21–23]. ISUP also has four grades: grade 1 with nucleoli inconspicuous or absent, grade2 with nucleoli not prominent but clearly visible at high-power magnification, grade 3 with prominent nucleoli, easily visualized at low-power magnification, and grade 4 with tumor giant cells present and/or marked nuclear pleomorphism [21–23].

Materials and methods

Patients

In this institutional review board-approved, Health Insurance Portability and Accountability Act-compliant study, we retrospectively queried our IRB approved and prospectively maintained surgical database for post-nephrectomy patients who had pathology proven ccRCC and who had preoperative multiphase CECT of the abdomen between June 2009 and June 2011. A total of 65 multiphase renal CT examinations with clear cell RCCs were utilized. 48 of the patients were male, and 17 were female. The mean age of the patients was 61.5 ± 12.1 years. There were 44 tumors with Fuhrman grades 1 or 2 (considered together) as well as 21 tumors with grades 3 or 4 (considered together). There were two primary reasons for considering grades 1 and 2 together, and grades 3 and 4 together: first, as discussed above, several studies have shown significant improvement in intra- and interobserver agreement among pathologists when the grading system is thus collapsed, and secondly, the distribution of cases in our sample was such that there were very few grade 1 and grade 4 cases.

CT examination

All CT examinations were performed with a 64-detector row helical CT scanner (Brilliance, Philips Healthcare, CT). The CT scans were obtained during patient breath-holding with the following parameters: 120 kVp, variable tube current, slice thickness of 0.5 mm with reconstruction interval of 2 mm. Non-contrast, arterial, nephrographic, and excretory phase images of the abdomen were obtained. Approximately 100–150 mL of non-ionic intravenous contrast material (Isovue 350; Bracco Imaging) dosed to weight was administered with a power injector at a rate of 5 mL/sec. Time delay to scanning for arterial phase images, nephrographic phase images, and excretory phase images were 25 s, 90 s, and 5 min, respectively. Arterial phase images were obtained rather than corticomedullary phase images to create a true arterial map for surgical planning. The arterial phase used in our study is essentially similar, however, a bit earlier than a corticomedullary phase. In our routine diagnostic workflow, we did not detect a difference in diagnostic quality with studies performed with arterial phase vs. corticomedullary phase for the patients who had both as comparisons.

Data processing

Multiphase CT acquisitions were transferred to a dedicated Synapse 3D workstation (Fujifilm Medical Systems

U.S.A., Stamford, CT). Renal tumor voxels were segmented manually, slice by slice, from surrounding voxels using Synapse 3D as 3D ROIs (Fig. 1), where segmentation refers to defining the area of interest voxel by voxel so that quantitative analysis is possible. Nephrographic phase of imaging was used for segmentation as it provided the clearest tumor demarcation. In only a few cases where the nephrographic phase did not provide adequate demarcation between the tumor and the normal parenchyma, other phases as well as the embedded edge detection software available in Synapse 3D were used. Additionally, the majority of tumors were at least partially exophytic, a feature which was also used to obtain the optimal segmentation. The affected kidney and tumor were segmented out in all phases to facilitate co-registration. The entire 3D tumor volume was chosen as the ROI—as opposed to subjectively selecting smaller subareas of the tumor in a 2D plane. There were several

reasons for this approach, with easier automated imaging processing workflow, accounting for tumor heterogeneity, simpler ROI definition, and improved reproducibility being the most important ones.

The DICOM-formatted CT images were converted into NIfTI (Neuroimaging Informatics Technology Initiative) volumes. NIfTI (http://nifti.nimh.nih.gov/) is a NIH-sponsored imaging initiative initially created to speed the development and enhance the utility of informatics tools related to neuroimaging. NIfTI is a file format which contains the entire imaged volume as well as a transformation which orients the voxels in three-dimensional scanner space. Given that it is just a file format representing voxels with no inherent knowledge about what the voxels contain, it is not constrained to a particular body part and can be used to convert any multi-file DICOM grayscale image into a single volumetric file.
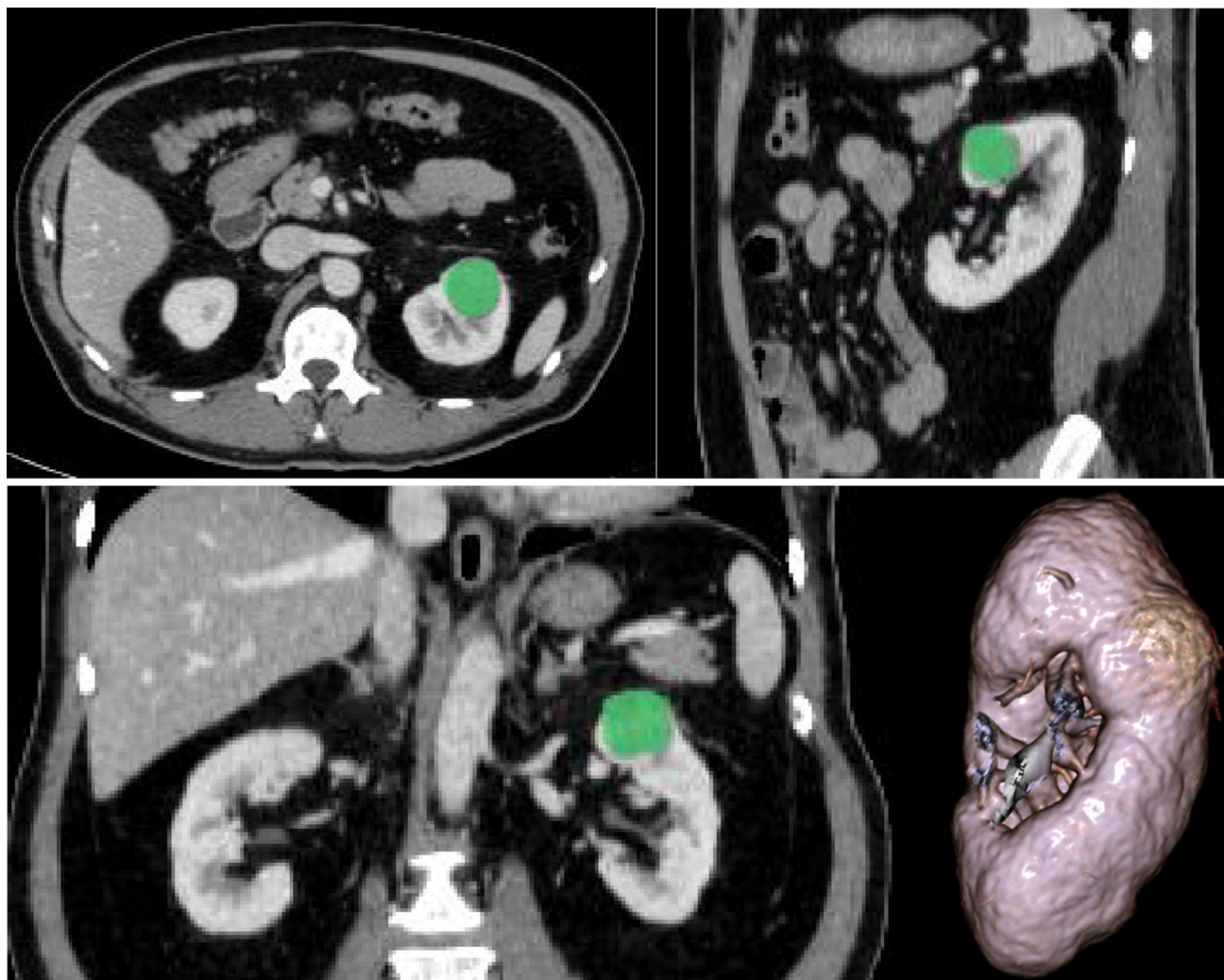

Fig. 1. The whole renal tumor is selected as a ROI. Reconstructions in axial, sagittal, and coronal planes show that the complete tumor is used for quantification. The rendered image display provides a visual reference and also references the total volume of the tumor analyzed.

DICOM keeps the images as individual slices, while NIfTI treats images as multidimensional volumes. The series of images were then co-registered using a Normalized Mutual Information (NMI) cost function implemented in Statistical Parametric Mapping SPM8 software package (The Wellcome Trust Centre for Neuroimaging at UCL, London, UK). NMI is a commonly used image similarity measure in image co-registration. A visual inspection of co-registered images was used to spot check for gross mis-registration. Custom MATLAB (MathWorks, Natick, MA) code was used to extract voxel data corresponding to the ROI.

Subsequently, histogram analysis of voxel data distribution was performed. Histogram mean, median, skewness, kurtosis, standard deviation, and interquartile range were extracted, using custom MATLAB analysis framework, for comparison between the 2 tumor grade groups for the following parameters: attenuation in each phase, absolute enhancement (arterial—pre-contrast), two washout parameters (arterial—nephrographic, arterial—excretory), and residual enhancement in nephrographic phase (nephrographic—pre-contrast) (Tables 1, 2).

While mean and median of parameter values are easily understood, the other histogram distribution parameters need further explanation. They are primarily ways to evaluate variance within a dataset. A more heterogeneous tumor would be expected to have greater variance, in other words, higher standard deviation and interquartile range, and lower kurtosis. Kurtosis is a measure of "peakedness" of histogram distribution,

skewness is a measure of asymmetry of histogram distribution, interquartile range is a measure of variability which is not as sensitive to outliers as standard deviation, and lastly standard deviation is a measure of degree of dispersion of attenuation values in a dataset.

Statistical analysis

In this work, Fuhrman grades 1 and 2 were considered together as low grade and Fuhrman grades 3 and 4 were considered together as high grade.

Statistical analysis was performed using SAS 9.4 (SAS Institute Inc., Cary, NC).

Data distribution was examined using D'Agostino-Pearson test, Anderson–Darling test, and histogram-based visual inspection.

Independent t test was used for normally distributed parameters; otherwise, Wilcoxon rank sum test was used. p values less than 0.05 were considered to indicate statistical significance.

Results

Tables 1 and 2 show the results of the histogram analysis of the parameter values discussed above for the lower grade tumors vs. the higher grade tumors.

Statistically significant difference was observed in four measured imaging parameters between grades 1–2 and grades 3–4: interquartile range of nephrographic phase attenuation, standard deviation of absolute

Table 1. Histogram analysis of attenuation values by phase of imaging, comparison between low-grade tumors and high-grade tumors

Parameter	Grade 1, 2, $N = 44$	Grades 3, 4, $N = 21$	p value
Non-contrast			
Kurtosis	2.38 ± 9.35	0.47 ± 2.33	0.7
Mean	27.44 ± 11.63	25.36 ± 6.55	0.72
Median	26.07 ± 10.73	24.26 ± 6.11	0.75
Interquartile range	126.45 ± 121.67	89.48 ± 47.88	0.18
Skewness	0.75 ± 0.99	0.45 ± 0.6	0.08
Standard deviation	15.8 ± 8.38	13.4 ± 5.1	0.26
Arterial phase			
Kurtosis	2.05 ± 9.2	1.01 ± 2.09	0.26
Mean	88.23 ± 35.27	84.76 ± 35.68	0.71
Median	87.76 ± 39.23	83.76 ± 37.4	0.7
Interquartile range	283.16 ± 130.78	254.1 ± 82.81	0.28
Skewness	0.47 ± 1.08	0.42 ± 0.53	0.81
Standard deviation	41.36 ± 13.8	35.6 ± 11.68	0.1
Nephrographic phase			
Kurtosis	1.58 ± 6.88	0.6 ± 1.33	0.51
Mean	114.51 ± 39.76	105.05 ± 29.42	0.35
Median	115.01 ± 44.07	103.43 ± 31.85	0.32
Interquartile range	292.86 ± 112.77	241.19 ± 39.22	0.02*
Skewness	0.19 ± 0.97	0.25 ± 0.64	0.52
Standard deviation	42.05 ± 9.09	36.88 ± 9.04	0.08
Excretory phase			
Kurtosis	31.49 ± 45.88	24.4 ± 43.41	0.56
Mean	77.67 ± 19.02	78.08 ± 21.44	0.94
Median	74.65 ± 20.08	72.9 ± 20.74	0.75
Interquartile range	523.52 ± 500.8	553.57 ± 592.48	0.83
Skewness	2.4 ± 3.03	2.29 ± 3.26	0.73
Standard deviation	34.75 ± 24.54	40.16 ± 31.48	0.53

Table 2. Histogram analysis of enhancement and washout parameters, comparison between low-grade tumors and high-grade tumors

Parameter	Grades 1, 2, $N = 44$	Grades 3, 4, $N = 21$	p value
Arterial—non-contrast			
Kurtosis	1.84 ± 8.97	1.14 ± 2.42	0.21
Mean	64.91 ± 40.12	62.89 ± 34.62	0.84
Median	63.77 ± 43.02	60.9 ± 35.79	0.79
Interquartile range	285.68 ± 111.43	252.52 ± 91.28	0.3
Skewness	0.46 ± 1.05	0.55 ± 0.57	0.16
Standard deviation	41.26 ± 11.56	34.66 ± 11.22	0.03*
Arterial—nephrographic			
Kurtosis	2.11 ± 4.13	3.32 ± 5.47	0.13
Mean	6.45 ± 42.95	16.93 ± 32.54	0.51
Median	3.07 ± 41.02	12.93 ± 31.25	0.48
Interquartile range	251 ± 137.79	206.95 ± 117.45	0.3
Skewness	0.86 ± 0.86	1.17 ± 0.83	0.12
Standard deviation	32.38 ± 12.68	27.03 ± 12.34	0.11
Arterial—excretory			
Kurtosis	8.1 ± 17.36	8.26 ± 20.63	0.69
Mean	30.49 ± 38.96	30.96 ± 39.43	0.96
Median	29.16 ± 36.83	29.05 ± 37.03	0.99
Interquartile range	443.95 ± 513.93	373.95 ± 519.48	0.16
Skewness	0.01 ± 2.17	0.24 ± 2.24	0.23
Standard deviation	41.57 ± 25.09	35.85 ± 24.91	0.16
Nephrographic—non-contrast			
Kurtosis	1 ± 4.68	0.44 ± 1.34	0.73
Mean	89.38 ± 41.7	81.44 ± 30.61	0.53
Median	89 ± 45.77	78.95 ± 32.86	0.48
Interquartile range	297.16 ± 109.47	235.57 ± 48.17	0.02*
Skewness	0.22 ± 0.78	0.37 ± 0.6	0.19
Standard deviation	42.45 ± 9.05	37.11 ± 7.86	0.04*

* p values are statistically significant (≤ 0.05)

enhancement (arterial—pre-contrast), as well as interquartile range and standard deviation of residual nephrographic enhancement (nephrographic—pre-contrast).

Standard deviation of absolute enhancement was 41.26 HU for grades 1–2 and 34.66 HU for grades 3–4 (p value 0.03) (Fig. 2).

Interquartile range of nephrographic phase attenuation was 292.86 HU for grades 1–2 and 241.19 HU for grades 3–4 (p value 0.02) (Fig. 3).

Interquartile range was 297.12 HU for residual nephrographic enhancement for grades 1–2 and 235.57 HU for grades 3–4 (p value 0.02), and standard deviation of the same was 42.45 HU for grades 1–2 and 37.11 HU for grades 3–4 (p value 0.04).

Discussion

Determining the Fuhrman nucleolar grade of a clear cell RCC has important management implications, especially in the context of active surveillance. Determining the Fuhrman grade and its evolutionary counterpart, the ISUP nucleolar grade, on pathologic evaluation, is the most commonly used method to prognosticate renal masses. The development of a non-invasive surrogate would add an additional tool in the management of patients with RCC. However, the development and validation of these metrics to classify the nucleolar grade is complicated given the interobserver variability of pathologic evaluations. In addition, tumors may be

heterogenous, and therefore, a single tumor may have loci of more than one tumor grade. Our results suggest that absolute enhancement is more heterogeneous for lower grade tumors and that residual enhancement in nephrographic phase is more heterogeneous for lower grade tumors.

Zhu et al. [24] retrospectively evaluated 255 patients with clear cell RCC and concluded that there was an inverse association between tumor enhancement and nuclear grade of RCC, with low tumor enhancement in the corticomedullary phase an independent predictor of high tumor grade. Our results demonstrated the same trend; however, it was not statistically significant. This may be partially due to sample size, but Zhu's study differs from ours in that they used subjectively selected smaller ROIs from 2D images, while in our study, the entire 3D tumor volume was defined as ROIs. As discussed above, our technique is subject to less interobserver variability and also accounts for heterogenous tumors. Other minor differences were that they used slower rate of contrast injection (3 vs. 5 mL/sec), and they used corticomedullary phase (30 s delay) vs. true arterial (25 s delay) as used in our study.

The negative correlation found between tumor grade and CT enhancement for clear cell RCC [24, 25] as well as for other tumors such as intrahepatic cholangiocarcinoma [26] has been reported to correlate with microvascular density of the tumors [24, 26]. Wang et al. established in their study of 24 cases of RCC that areas
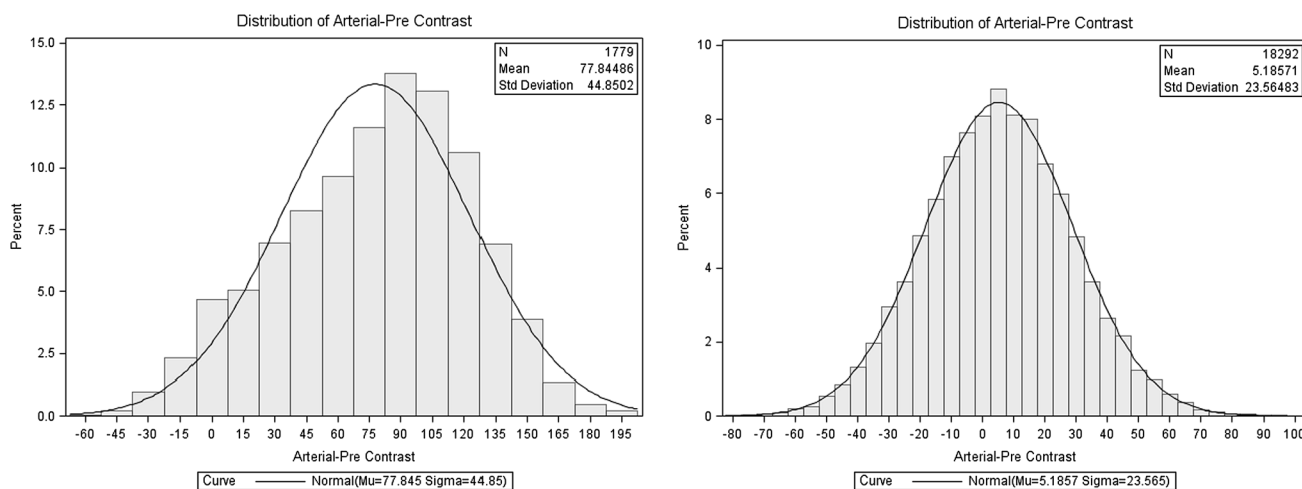
Fig. 2. Statistically significant difference was observed in standard deviation of absolute enhancement (arterial—pre-contrast). *Left graph* an example grade 2 RCC, SD 45 HU, *right graph* an example grade 3 RCC, SD 24.
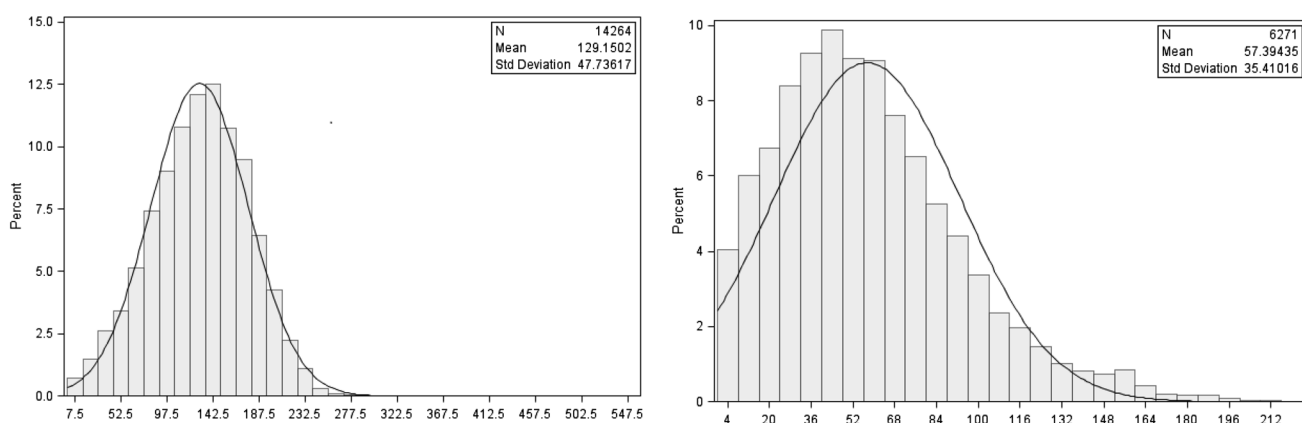

Fig. 3. Statistically significant difference was observed in interquartile range for nephrographic phase attenuation. *Left graph* an example grade 2 RCC, nephrographic phase interquartile range 549, *right graph* an example grade 3 RCC, nephrographic phase interquartile range 219.

of higher microvascular density resulted in higher CT enhancement [27]. Combining the results of Wang et al. and Zhu et al., a possible but unproven explanation is that lower grade tumors may have higher microvascular density. It is conceivable this higher microvascular density of lower grade tumors then results in more heterogeneous absolute enhancement as well as more heterogeneous residual enhancement in nephrographic phase, as suggested by our results. These possible explanations, however, need further validation. Given the importance of developing quantitative models to predict Fuhrman grade of RCC, this is an important first step in devising a predictive model. Quantifiable physical parameters including a shape and volume analysis as well as texture analysis could provide more diagnostic information.

There are several limitations to this study. This was a single-center retrospective study, and the results ideally need to be validated in a prospective multicenter trial. However, the straightforward definition of the ROI used in this study, viz. the entire 3D tumor volume, should make reproduction of the results at another center possible. Another limitation of this study was that we did not have a quantitative algorithm available to account for the degree or amount of necrosis; we are in fact evaluating such a feature currently. It is known that the amount or degree or necrosis does correlate with a higher grade of tumors and worse prognosis [28, 29]. Lastly, the sample size of our study was relatively small.

Conclusions

This study demonstrated statistically significant difference in four of the parameters characterizing contrast enhancement and washout between lower grade and higher grade tumors, viz. interquartile range of nephro-

graphic phase attenuation, standard deviation of absolute enhancement, as well as interquartile range and standard deviation of residual nephrographic phase enhancement.

Our results suggest that absolute enhancement and residual enhancement in nephrographic phase are both more heterogeneous for lower grade tumors.

Given the importance of developing quantitative model to predict the nucleolar grade, this is an important step in coming up with a non-invasive model.

Author contributions. Hannu Huhdanpaa—primary author of the paper, data processing and analysis; Darryl Hwang—development of Matlab algorithms for data processing; Steven (Yong) Cen—statistical analysis; Brian Quinn—segmenting and registering data; Megha Nayyar—segmenting and organizing data; Xuejun Zhang—Algorithm development and review; Frank Chen—reviewing data and image analysis; Bhushan Desai—drafting, coordination, and statistical review; Gangning Liang—pathological correlation; Inderbir Gill—clinical correlation and analysis; and Vinay Duddalwar—primary radiology faculty mentor, overall guidance, coordination, and review.

Disclosure. Hannu Huhdanpaa, Darryl Hwang, Steven (Yong) Cen, Brian Quinn, Megha Nayyar, Xuejun Zhang, Frank Chen, Bhushan Desai, Gangning Liang, Inderbir Gill, Vinay Duddalwar have nothing to disclose.

References

1. Cho E, Adami HO, Lindblad P (2011) Epidemiology of renal cell cancer. Hematol Oncol Clin N Am 25:651–665
2. Gandaglia G, Ravi P, Abdollah F, et al. (2014) Contemporary incidence and mortality rates of kidney cancer in the United States. Can Urol Assoc J 8:247–252
3. Hock LM, Lynch J, Balaji KC (2002) Increasing incidence of all stages of kidney cancer in the last 2 decades in the United States: an analysis of surveillance, epidemiology and end results program data. J Urol 167:57–60
4. Gill IS, Aron M, Gervais DA, Jewett MA (2010) Clinical practice. Small renal mass. N Engl J Med 362:624–634
5. Donat SM, Diaz M, Bishoff JT, et al. (2013) Follow-up for clinically localized renal neoplasms: AUA guideline. J Urol 190:407–416
6. Sheir KZ, El-Azab M, Mosbah A, El-Baz M, Shaaban AA (2005) Differentiation of renal cell carcinoma subtypes by multislice computerized tomography. J Urol 174:451–455 ((discussion 455))
7. Zhang J, Lefkowitz RA, Ishill NM, et al. (2007) Solid renal cortical tumors: differentiation with CT. Radiology 244:494–504
8. Herts BR, Coll DM, Novick AC, et al. (2002) Enhancement characteristics of papillary renal neoplasms revealed on triphasic helical CT of the kidneys. AJR Am J Roentgenol 178:367–372
9. Jinzaki M, Tanimoto A, Mukai M, et al. (2000) Double-phase helical CT of small renal parenchymal neoplasms: correlation with pathologic findings and tumor angiogenesis. J Comput Assist Tomogr 24:835–842
10. Kim JK, Kim TK, Ahn HJ, et al. (2002) Differentiation of subtypes of renal cell carcinoma on helical CT scans. AJR Am J Roentgenol 178:1499–1506
11. Press GA, McClennan BL, Melson GL, et al. (1984) Papillary renal cell carcinoma: CT and sonographic evaluation. AJR Am J Roentgenol 143:1005–1009
12. Ruppert-Kohlmayr AJ, Uggowitzer M, Meissnitzer T, Ruppert G (2004) Differentiation of renal clear cell carcinoma and renal papillary carcinoma using quantitative CT enhancement parameters. AJR Am J Roentgenol 183:1387–1391
13. Lee-Felker SA, Felker ER, Tan N, et al. (2014) Qualitative and quantitative MDCT features for differentiating clear cell renal cell carcinoma from other solid renal cortical masses. AJR Am J Roentgenol 203:W516–W524
14. Fuhrman SA, Lasky LC, Limas C (1982) Prognostic significance of morphologic parameters in renal cell carcinoma. Am J Surg Pathol 6:655–663
15. Bektas S, Bahadir B, Kandemir NO, et al. (2009) Intraobserver and interobserver variability of Fuhrman and modified Fuhrman grading systems for conventional renal cell carcinoma. Kaohsiung J Med Sci 25:596–600
16. Al-Aynati M, Chen V, Salama S, et al. (2003) Interobserver and intraobserver variability using the Fuhrman grading system for renal cell carcinoma. Arch Pathol Lab Med 127:593–596
17. Ficarra V, Martignoni G, Maffei N, et al. (2005) Original and reviewed nuclear grading according to the Fuhrman system: a multivariate analysis of 388 patients with conventional renal cell carcinoma. Cancer 103:68–75
18. Lang H, Lindner V, de Fromont M, et al. (2005) Multicenter determination of optimal interobserver agreement using the Fuhrman grading system for renal cell carcinoma: assessment of 241 patients with >15-year follow-up. Cancer 103:625–629
19. Sun M, Lughezzani G, Jeldres C, et al. (2009) A proposal for reclassification of the Fuhrman grading system in patients with clear cell renal cell carcinoma. Eur Urol 56:775–781
20. Qayyum T, McArdle P, Orange C, et al. (2013) Reclassification of the Fuhrman grading system in renal cell carcinoma-does it make a difference? Springerplus 2:378
21. Delahunt B, McKenney JK, Lohse CM, et al. (2013) A novel grading system for clear cell renal cell carcinoma incorporating tumor necrosis. Am J Surg Pathol 37:311–322
22. Delahunt B, Egevad L, Montironi R, Srigley JR (2013) International Society of Urological Pathology (ISUP) consensus conference on renal neoplasia: rationale and organization. Am J Surg Pathol 37:1463–1468
23. Delahunt B, Cheville JC, Martignoni G, et al. (2013) The International Society of Urological Pathology (ISUP) grading system for renal cell carcinoma and other prognostic parameters. Am J Surg Pathol 37:1490–1504
24. Zhu YH, Wang X, Zhang J, et al. (2014) Low enhancement on multiphase contrast-enhanced CT images: an independent predictor of the presence of high tumor grade of clear cell renal cell carcinoma. AJR Am J Roentgenol 203:W295–W300
25. Villalobos-Gollás M, Aguilar-Davidov B, Culebro-García C, et al. (2012) Pathological implications of areas of lower enhancement on contrast-enhanced computed tomography in renal-cell carcinoma: additional information for selecting candidates for surveillance protocols. Int Urol Nephrol 44:1369–1374
26. Nanashima A, Abo T, Murakami G, et al. (2013) Intrahepatic cholangiocarcinoma: relationship between tumor imaging enhancement by measuring attenuation and clinicopathologic characteristics. Abdom Imaging 38:785–792
27. Wang JH, Min PQ, Wang PJ, et al. (2006) Dynamic CT evaluation of tumor vascularity in renal cell carcinoma. AJR Am J Roentgenol 186:1423–1430
28. Sengupta S, Lohse CM, Leibovich BC, et al. (2005) Histologic coagulative tumor necrosis as a prognostic indicator of renal cell carcinoma aggressiveness. Cancer 104:511–520
29. Knight DA, Stadler WM (2007) Prognostic factors in localized renal cancer. BJU Int 99:1212–1216